Hindawi
Advances in Materials Science and Engineering
Volume 2022, Article ID 3000233, 15 pages
https://doi.org/10.1155/2022/3000233

Research Article

Statistical Modeling and Optimization of Laser Cladding Stellite 6/WC Composite Coating

Teng Wu,[1] Wenqing Shi,[1] Linyi Xie,[1] Meimei Gong,[1] Jiang Huang,[1] Yuping Xie,[1] and Kuanfang He[2]

[1]*College of Electronics and Information Engineering, Guangdong Ocean University, Zhanjiang 524088, China*
[2]*School of Mechatronic Engineering and Automation, Foshan University, Foshan 528000, China*

Correspondence should be addressed to Wenqing Shi; swqafj@126.com

Received 15 November 2021; Revised 28 December 2021; Accepted 4 May 2022; Published 25 May 2022

Academic Editor: David Holec

A response surface was employed to establish a statistical model for influencing factors and response targets to study the influence of laser cladding process parameters on the quality of Co-based WC composite coating and reduce defects in the cladding layer. Analysis showed that the cladding step and laser power were the most significant factors affecting the coating's porosity area and surface flatness. Increasing the amount of WC and the laser power significantly enhanced the hardness of the coating. The validation experiments under optimized conditions showed that the predicted value of the model was in good agreement with the actual value, and the average error was less than 6%. This study presents the preparation of Co-based WC ceramic composite coating by laser cladding and the optimization of process parameters.

1. Introduction

In recent years, modern surface modification methods and technologies make it possible for components to meet performance requirements under different working conditions [1]. Laser cladding is an advanced surface modification technique, and the cladding material and the base material surface melt at the same time, so the cladding layer and the substrate combine metallurgically. It is widely used in agricultural machinery and product performance improvement and repair, etc., because of the high density of laser energy, fast heating, and the advantages of small deformation, surface coating often alters or improves the performances of materials [2–6].

In general, in the process of laser cladding preparation, the quality control of the cladding layer is a key issue for the expansion and application of laser cladding technology. For example, poor formation and low hardness of the cladding layer are largely attributed to the improper selection of laser cladding process parameters. To solve this problem, there has been detailed research on process parameter optimization. Zhao et al. [7] designed 125 groups of experiments using the single-factor method and discussed the effect of process parameters on the geometric morphology of a single YCF104 cladding layer by variance analysis. Shu et al. [8], by combining single-factor and multi-factor orthogonal experiments, successfully found optimal process parameters for the preparation of 304L coating by laser cladding. It can be seen from the above investigations that, to ascertain the relationship between process parameters and coating quality, researchers need to conduct a large number of experimental studies. Therefore, it is necessary to establish a prediction model for the relationship between the process parameters and coating quality. De Hosson [9] and Onwubolu et al. [10] proposed an empirical formula that can describe the relationship between laser process parameters and cladding layer geometry. Liu et al. [11] verified this empirical formula by experiments. Their results showed that the predicted values had certain reference values for the experimental measurements. Khorram et al. [12] used the response surface methodology to establish a statistical model between the input variables (laser frequency, pulse width,

and scanning speed) and the output response (cladding width, height, cladding angle, dilution rate, and hardness). The regression equation between the process parameters and the quality of the cladding layer was obtained. After parameter optimization and experimental verification, the error between the predicted value and the actual value was 11.4%. Ma et al. [13] optimized the process parameters of AlSi10 Mg alloy by the Taguchi method and the variance analysis method so that the prediction accuracy of the model was improved to 99%.

However, the above literature mainly evaluates the geometric morphology and quality of the single-track cladding layer based on process parameters and combined parameters. In practical production and applications, when repairing large components or large-scale cladding on the surface of a workpiece, the use of single-track laser cladding is limited, and multitrack cladding is needed. Due to the concentration of laser energy, the material can melt rapidly in the cladding process. Also, because of the small heating area and short solidification time, the pores generated during the cladding forming cannot overflow, thus forming pores [14, 15]. An increased porosity area will reduce the mechanical properties of the coating, and it also causes local stress concentration near the pores, resulting in cracks [16]. Compared with single-pass cladding, multipass cladding has to account for not only the stomatal area but also the influence of the cladding step between adjacent cladding layers and other parameters on the surface flatness. In addition, current research on metal matrix composite coatings mainly focuses on molecular dynamics simulation [17–19], coating preparation methods [20–22], multilayer coatings [23], coating properties [24], and so on. In the process of coating preparation, there are few reports on the defects (pores, surface flatness) controlling the composite coating.

Therefore, to solve the problems of surface collapse and pores in the cladding layer in the process of cermet composite coating on a 60Si2Mn surface by laser cladding in this study, a Co-based WC composite cladding layer was prepared on a 60Si2Mn matrix. The response surface method (RSM) was used to construct a mathematical model of laser process parameters (laser power, scanning speed, cladding step, WC content) and cladding layer quality (porosity area, surface flatness, cladding layer hardness). The variance analysis method was used to reveal the influence of each influencing factor on the response target. Finally, the optimal process parameters of laser cladding Co-based WC coating were obtained through optimization verification.

2. Experiment

2.1. Experimental Materials and Equipment. In the experiment, 60Si2Mn was selected as the matrix material, with a hardness of 255.1$HV_{0.2}$ and dimensions of 50 mm (length) × 40 mm (width) × 3 mm (thickness). Table 1 shows the chemical composition of the matrix material. Stellite 6 (manufactured by the Nangong Xindun Alloy Welding Material Spraying Co., Ltd) was used as the cladding material. WC (manufactured by the Nangong Xindun Alloy Welding Material Spraying Co., Ltd) ceramic powder (purity 99.8%) was added to the Co-based alloy powder with a mass fraction of 0%, 15%, and 30%, respectively. Table 2 shows the chemical composition of the cladding powder.

A fiber laser processing system (XL-F2000 T) was selected as the laser cladding system, which mainly comprises the cooling unit, laser, CNC control system, laser cladding head, moving execution system, processing workbench, etc., as shown in Figure 1. The laser beam wavelength was 1080 ± 5 nm, the defocusing distance was 5 mm, and the spot diameters of the laser beam acting on the surface of the substrate were 622 μm (LP: 500 W), 790 μm (LP: 600 W), and 894 μm (LP: 700 W). The principle of laser cladding is to add cladding material to the surface of the substrate and then use a high-energy density laser beam to melt this thin layer together with the surface of the substrate, so as to form a metallurgically combined cladding layer on the surface of the substrate.

2.2. Experimental Method and Scheme Design. The response surface is an analysis method combining experimental design and mathematical modeling that can demonstrably reflect the effect of various influencing factors and combined factors on the response target value in an experimental process. By obtaining the regression equation of various factors on the response value, the prediction of the target value and the optimization of the factor level can be realized [10, 25]. Equation (1) is a second-order regression equation for constructing the mathematical model [26], and equation (2) is a multiobjective optimization equation [27].

$$y = b_0 + \sum_{i=1}^{k} b_i x_{iu} + \sum_{i=1}^{k} b_{ii} x_{iu}^2 + \sum_{i<j}^{k} b_{ij} x_{iu} x_{ju} + \varepsilon, \quad (1)$$

where y is the response target; x is an independent input variable; k is the factor number; u is the experimental design number; b_0, b_i, b_{ii}, and b_{ij} are regression coefficients, respectively, and ε is the error.

$$\text{Desirability} = \left(\prod_{i=1}^{n} d_i^{r_i} \right)^{1/\sum r_i}, \quad (2)$$

where d_i is the satisfaction function of each predicted response, n is the number of responses, and r_i is the weight of the response.

In the process of laser cladding, many process parameters are involved, including the laser power (LP), the scanning speed (V), the cladding step (CSD), and the amount of tungsten carbide (WCC), that affect the quality of the cladding layer (porosity area, surface flatness, and hardness) [28–30]. A trial-and-error investigation was carried out before the formal start of the experiment in order to select the range of process parameters. Therefore, the experimental scheme was designed based on the Box–Behnken design (BBD), using the operating interface of the Design-Expert v11 response surface software. Four process parameters, including the laser power, the scanning speed, the cladding step, and the amount of WC powder,

Table 1: Chemical composition of the 60Si2Mn plate (mass fraction, %).

Specification	C	Si	Mn	Ni	Cu	Cr	P	S
60Si2Mn	0.56–0.6	1.5–2.0	0.6–0.9	≤0.35	≤0.25	≤0.35	≤0.035	≤0.035

Table 2: Chemical composition of Stellite 6 powder (mass fraction, %).

Specification	C	Cr	Si	W	Fe	Mo	Ni	Co	Mn
Stellite 6	1.15	29.00	1.10	4.00	3.00	1.00	3.00	Bal	0.50

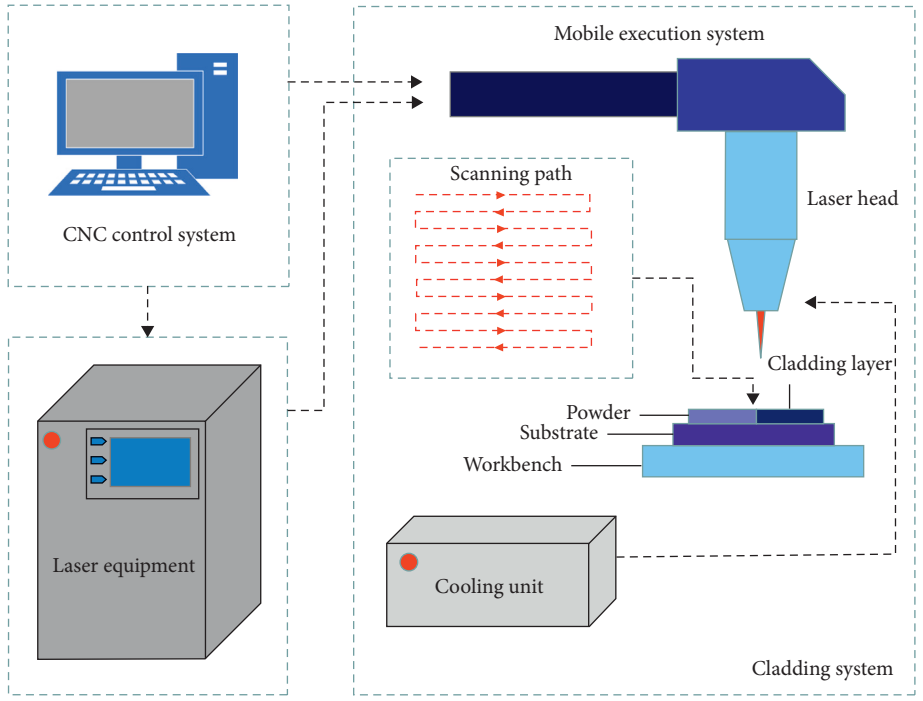

Figure 1: The laser cladding system.

were selected as influencing factors, and three levels were selected for each factor. Table 3 shows the laser process parameters and the horizontal design. The porosity area, the surface flatness, and the hardness of the cladding layer were selected as the response target values, and 29 groups of experiments were designed using the BBD scheme, as shown in Table 4.

Before laser cladding, the substrate was polished with sandpaper of different grades and cleaned with anhydrous ethanol to remove surface impurities. Then, the substrate and cladding powder were put into a drying oven to dry. The powder was prepared by prefabrication with a laying thickness of about 1 mm. After the cladding was completed, 29 groups of samples were cut, prepared, and polished, to obtain the cross-sectional morphology of the cladding layer shown in Figure 2. The Image J software was used to measure the surface flatness and porosity area of the cladding layer, and the microhardness of the cladding layer was measured with a Vickers hardness tester (MHVD-1000AT). The average value was taken, the loading load was 200 gf, and the load-holding time was 10 s. Figure 3 shows the surface flatness and hardness indentation of the cladding layer.

3. Results and Discussion

3.1. Establishing the Response Target Mathematical Model. Using the Design-Expert v11 software, the BBD design scheme was used to build mathematical models of the porosity area, the surface flatness, and the hardness of the cladding layer, and the fitting regression equations of each model were obtained, as shown in the following equations:

$$\begin{aligned} S_{coded} &= 17,1500 - 62,269 \times LP + 84,746 \times CSD \\ &\quad - 136,800 \times V \times WCC, \\ F_{coded} &= 0.3772 - 0.0811 \times LP + 0.0641 \times CSD, \\ HV_{coded} &= 423 + 30 \times LP - 17 \times V + 133 \times WCC \\ &\quad + 29 \times LP^2 + 25 \times CSD^2 + 28 \times WCC^2, \end{aligned} \tag{3}$$

Table 3: Laser process parameters and the level design.

Level	LP (W)	V (mm/min)	CSD (mm)	WCC (%)
−1	500	200	0.7	0
0	600	300	0.9	15
1	700	400	1.1	30

Table 4: BBD experimental scheme design and results.

Standard order	Factors				Responses		
	LP (W)	V (mm/min)	CSD (mm)	WCC (%)	Porosity area (μm^2)	Flatness (mm)	Hardness (HV 0.20)
1	500	200	0.9	15	203579	0.45	453.76
2	700	200	0.9	15	89734	0.25	525
3	500	400	0.9	15	206924	0.418	412.63
4	700	400	0.9	15	107078	0.437	458.1
5	600	300	0.7	0	73851	0.294	337.43
6	600	300	1.1	0	150586	0.415	331.56
7	600	300	0.7	30	229906	0.29	639.5
8	600	300	1.1	30	269434	0.353	590.8
9	500	300	0.9	0	114267	0.636	331.8
10	700	300	0.9	0	46938.3	0.44	361.4
11	500	300	0.9	30	224470	0.412	568.23
12	700	300	0.9	30	123786	0.19	675.9
13	600	200	0.7	15	61432.2	0.161	496.6
14	600	400	0.7	15	55752.4	0.259	459.8
15	600	200	1.1	15	337432	0.34	462.1
16	600	400	1.1	15	399788	0.545	431.5
17	500	300	0.7	15	128456	0.526	421.9
18	700	300	0.7	15	35627.6	0.265	458.78
19	500	300	1.1	15	358719	0.512	471.4
20	700	300	1.1	15	86020	0.399	536.3
21	600	200	0.9	0	55488	0.17	319.9
22	600	400	0.9	0	378219	0.4	351.6
23	600	200	0.9	30	347688	0.308	605.67
24	600	400	0.9	30	123334	0.24	550.96
25	600	300	0.9	15	189734	0.3	403.2
26	600	300	0.9	15	134855	0.556	450.6
27	600	300	0.9	15	202847	0.35	419.45
28	600	300	0.9	15	72048.1	0.417	428.16
29	600	300	0.9	15	257960	0.263	411.73

where S_{coded}, F_{coded}, and HV_{coded} are the fitting regression equations of the porosity area, the surface flatness, and the hardness, respectively.

3.2. Analysis of the Porosity Area of the Cladding Layer. The model analysis mostly included the variance and the residual error. The main purpose of ANOVA was to determine whether the interaction between the influencing factors had a significant impact on the response target and to explain the model. Residual analysis showed the fitting accuracy and the prediction effect of the model more intuitively. Then, the perturbation method, contour plots, and three-dimensional response curves were used to analyze the relationship between each factor and its interaction terms and the response values. It should be noted that to further ensure the accuracy of the model, nonsignificant terms were eliminated in the fitting process of the regression equation; that is, $P > 0.05$, where P is the significance probability.

3.2.1. Porosity Area Variance and Residual Analysis. The mathematical model of the porosity area was tested by ANOVA and residual analysis. As can be seen from the results of ANOVA in Table 5, the P value of the model coefficient was 0.0078, which was less than 0.05, indicating that the model was significant, and only 0.78% of the probability would be distorted due to interference factors. The P value of the lack-of-fit coefficient was 0.5612, higher than the critical value of 0.05, indicating that this model can better describe the influence of process parameters on the porosity area. In addition, the determination coefficient R^2 was close to 1, which shows that the experimental results are closely related to the porosity area prediction model, and the effective signal-to-noise ratio (Adeq Precision) is greater than 4, which indicates that the regression model of porosity area is accurate. By comparing the P values of each factor, it was found that the cladding step had the greatest effect on the porosity area of the cladding layer, followed by the laser power. The influence of the WC content of the porosity area

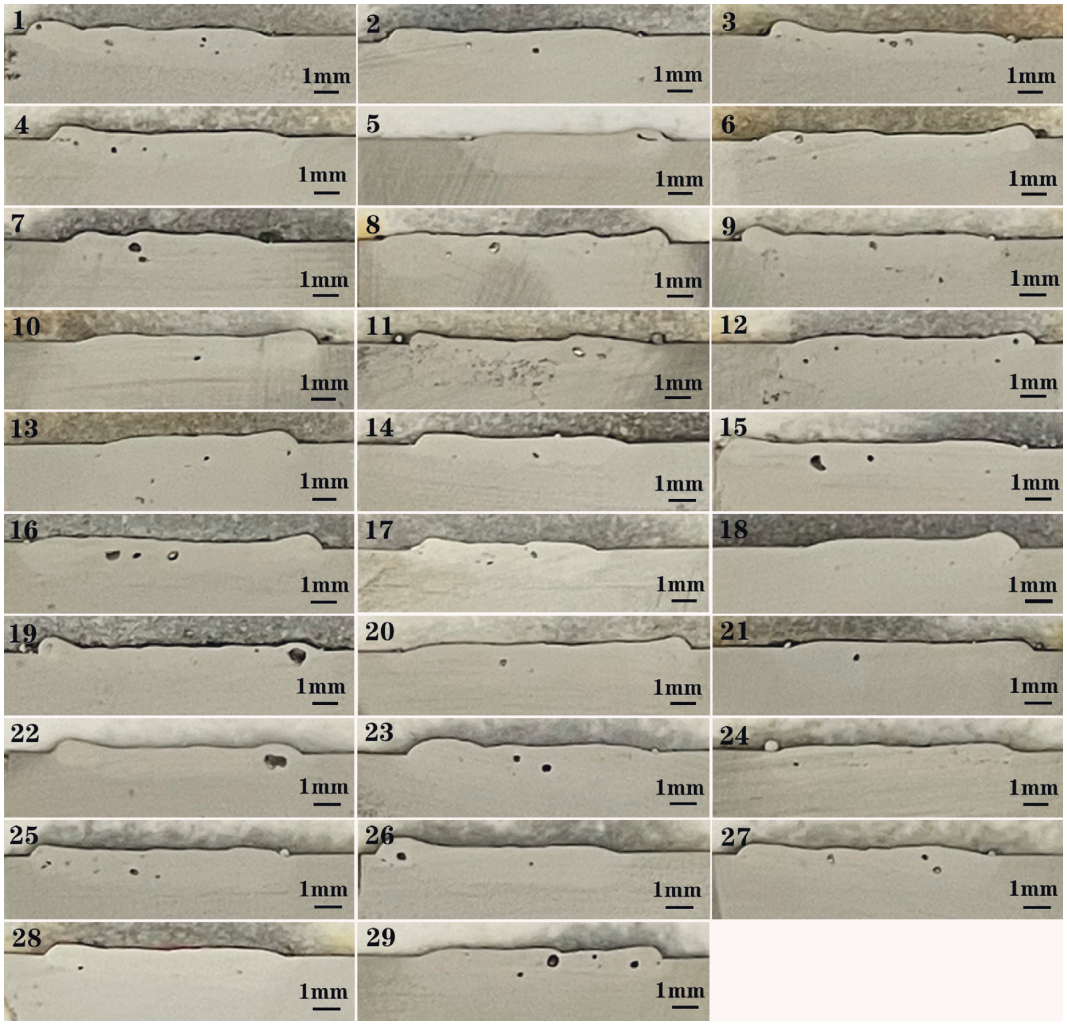

Figure 2: Cross-sectional morphology of the cladding layer.

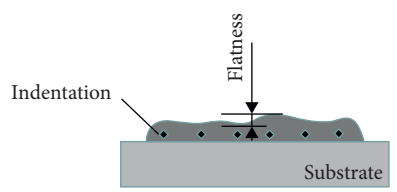

Figure 3: The surface flatness and hardness indentation of the cladding layer.

Table 5: Variance analysis of the porosity area of the cladding layer.

Source	Sum of squares	df	Mean square	F	P	
Model	2.684×10^{11}	14	1.917×10^{10}	3.9100	0.0078	Significant
LP	4.653×10^{10}	1	4.653×10^{10}	9.4800	0.0082	
V	2.574×10^{09}	1	2.574×10^{09}	0.5244	0.4809	
CSD	8.618×10^{10}	1	8.618×10^{10}	17.5600	0.0009	
WCC	2.077×10^{10}	1	2.077×10^{10}	4.2300	0.0588	
$V \times$ WCC	7.483×10^{10}	1	7.483×10^{10}	15.2500	0.0016	
Residual	6.871×10^{10}	14	4.908×10^{09}			
Lack of fit	4.868×10^{10}	10	4.868×10^{09}	0.9725	0.5612	Not significant
Pure error	2.002×10^{10}	4	5.006×10^{09}			
Correlation total	3.371×10^{11}	28				
R^2	0.7962			Adeq Precision	7.0809	

was small, and the scanning speed had no significant effect on it. However, the interaction terms between the scanning speed and the WC content had a significant effect on the porosity area. Therefore, combined with the mean square value, the primary and secondary order of the process parameters affecting the size of the porosity area was CSD > LP > WCC > V.

Figure 4 is the diagnosis diagram of the porosity area model. According to Figure 4(a), the normal probability distribution of the residuals is approximately a straight line, and most residual values are concentrated in the middle of the line, indicating that the residual distribution of this model is normal. In Figure 4(b), the predicted values of the model are consistent with the real values measured in the experiment, and the prediction accuracy is good. Figure 4(c) shows that there is no specific mathematical relationship between the residual value and the predicted value, and the residual value is randomly distributed. As shown in Figure 4(d), it was found that the residuals were randomly distributed in the order of observation, but no specific relationship between the order of observation and the residuals was found. The residuals were all distributed around the 0 value, indicating that there were no outliers in the order of observation. In conclusion, the model of the porosity area is reliable, the prediction accuracy is high, and the model has good adaptability.

3.2.2. Influence of the Laser Process Parameters on the Porosity Area. Figure 5 shows the perturbation of the process parameters on the porosity area. It shows that with an increase in the laser power, the porosity area decreased. This is because the higher the power, the higher the energy received by the cladding layer per unit area, the stronger the convection of the molten pool, the longer the duration, and some bubbles have sufficient time to overflow, so the porosity area decreases. With an increase in the scanning speed, the pore area increased correspondingly, which is consistent with previous research [31], because increasing the scanning speed will shorten the liquid life of the molten pool, the powder of the cladding layer is not fully stirred, and the time required for bubbles to float to the surface of the cladding layer is longer than the liquid life of the molten pool, resulting in an increase in the porosity area of the cladding layer. There is a positive correlation between the cladding step and the porosity area. When the cladding step is small, the remelting area of the multichannel lap is relatively large, and some bubbles in the remelting area can overflow, thus reducing the porosity area of the cladding layer, with an increase in the cladding step distance, the overlapping rate, and remelting area decrease, and bubbles remaining in the cladding layer increase, which leads to an increase in the porosity area. The porosity area increases with an increase in the WC ceramic powder, because, as shown in Figure 6, an increase in the WC powder content in the cladding layer will lead to an increase in the coating height, which will make the path of bubbles from the bottom of the coating to the surface longer. The pores are thus not able to fully overflow, and the porosity area increases.

Figure 7 shows the influence of the interaction between the laser power and the cladding step on the porosity area. It can be intuitively seen from Figures 7(a) and 7(b) that the porosity area of the cladding layer formed by high power and a small cladding step is relatively small, and vice versa. A large number of pores will lead to cracks or other structural defects. Therefore, to improve the quality of the cladding coating and inhibit an increase in the porosity area, higher power and a smaller cladding step were selected in the subsequent optimization process.

3.3. Surface Flatness Analysis

3.3.1. Surface Flatness Variance and Residual Analysis. As can be seen from the results of the variance analysis in Table 6, the F and P values for this model are 2.59 and 0.0429, respectively, indicating that the model is significant. The F value of the lack of fit is 0.4578, which means that the lack of fit is not significant relative to the pure error, and the model can be fitted. R^2 is 0.7215, indicating that the fitting accuracy and prediction effect of the constructed surface flatness model are good. A value of Adeq Precision greater than 4 is desirable, proving that the signal is sufficient. According to the F and P values of the process parameters, the factors affecting the significance of surface flatness, from high to low, are LP > CSD > V > WCC.

Figure 8 presents the diagnostic graphs of the surface flatness model. As can be seen from Figure 8(a), the general trend of the experimental sample points in the graph is obviously a straight line, indicating that the hypothesis of normality of error is reasonable. As can be seen from Figure 8(b), the error between the actual measured data and the predicted values of the model is small, indicating that the constructed mathematical model can describe the influence of the laser processed parameters on the surface flatness well. In Figure 8(c), the residuals are distributed in a decentralized and irregular manner, and there are no abnormal points near the regression line, indicating good adaptability of the model and a reasonable range of selected process parameters. As can be seen from Figure 8(d), there are no outliers in the measured 29 groups of experimental sample points. The difference between the observed values and the predicted values is above and below the horizontal line with a value of 0, which indicates that the model has high accuracy and good reliability.

3.3.2. Influence of the Laser Process Parameters on the Surface Flatness. Figure 9 reveals the influence of the laser process parameters on the surface flatness of the cladding layer. The results show that the surface flatness decreased with increasing laser power. This is because as the laser power increases, the peak laser energy density increases, and the heat in the substrate and the cladding layer is also higher. As a result, the size of the molten pool and lap joint increases, thus increasing the remelting area of the cladding layer, and remelting reduces the bulge height of the coating edge to some extent, resulting in a decrease in the surface flatness. The scanning speed affects the height of surface flatness.

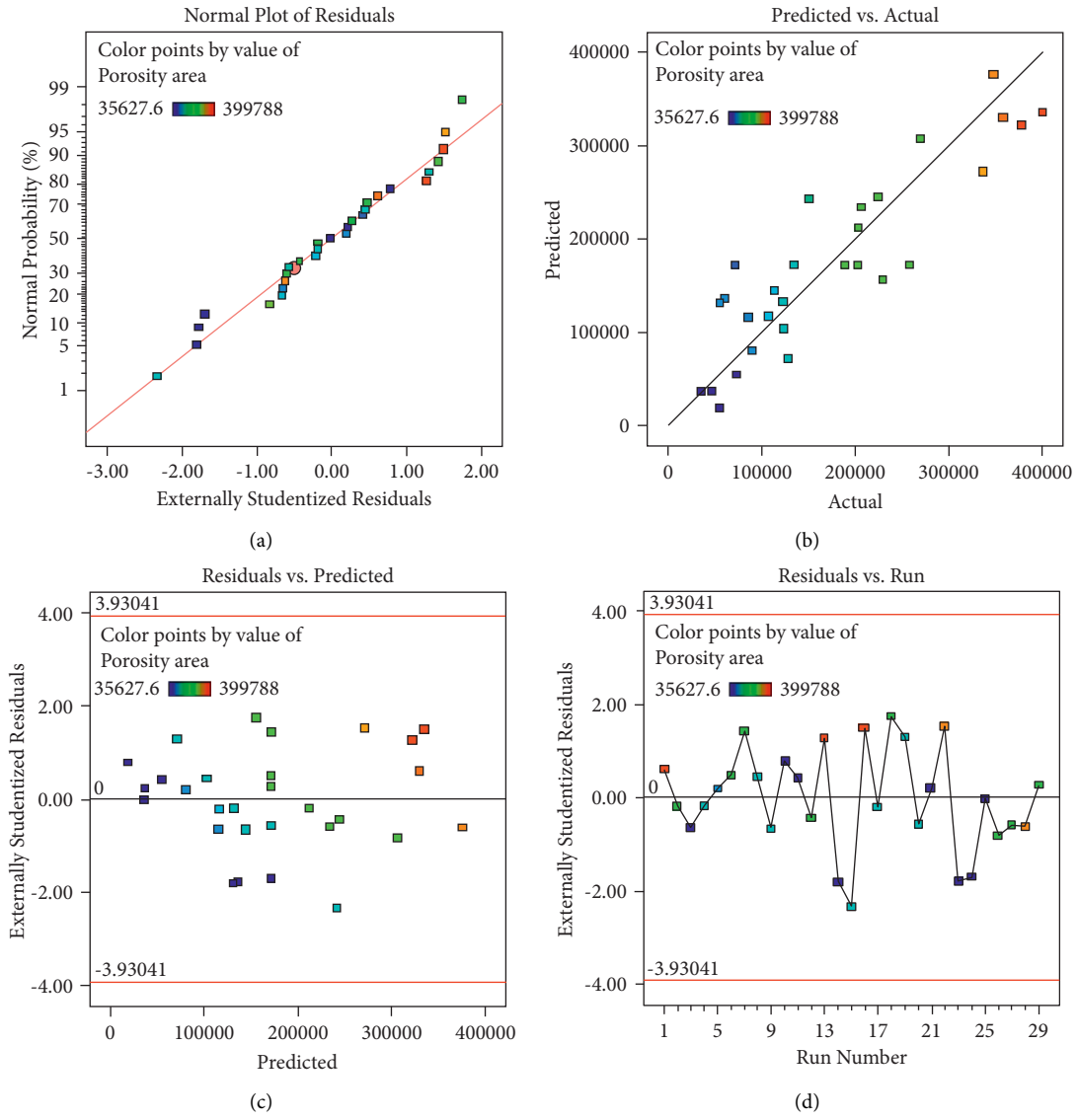

Figure 4: Diagnostic diagram of the porosity area model: (a) the normal distribution of the residuals; (b) projected and actual values; (c) predicted values and residuals; (d) serial number and residuals.

When the scanning speed is low, the unit time of the laser beam acting on the cladding layer increases. As a result, the heat of the cladding layer increases, more cladding powder melts, and the cladding area increases, Under the action of surface tension and gravity, the surface flatness of the coating decreases as a consequence. With an increase in the cladding step, the overlapping rate decreases, and the remelting area at the lap joint decreases, which leads to an obvious depression between adjacent cladding channels, thus increasing the height difference. The surface flatness decreases with an increase in the WC powder content. Research shows that WC particles aggregate heated, then slowly release heat, reducing the curing rate of the coating [32]. Therefore, the heat absorbed by the coating increases, and its fluidity increases. The coating in the molten state, therefore, has a leveling trend.

From the contour diagram and the three-dimensional response curve diagrams (Figure 10), we can see the influence of the interaction between laser power and cladding step on the surface flatness and draw the conclusion that, when the laser power is 700 W and the cladding step distance is 0.7 mm, the flatness of the multichannel lap Co-based WC composite coating formed was the lowest.

3.4. Hardness Analysis of the Cladding Layer

3.4.1. Analysis of the Hardness Variance and the Residuals of the Cladding Layer. Table 7 shows the variance analysis table of the cladding layer hardness. The results show that this model is of high significance, the lack of fit is not significant relative to the pure error, and the fitting and prediction accuracy are high. Increasing the WC powder content for

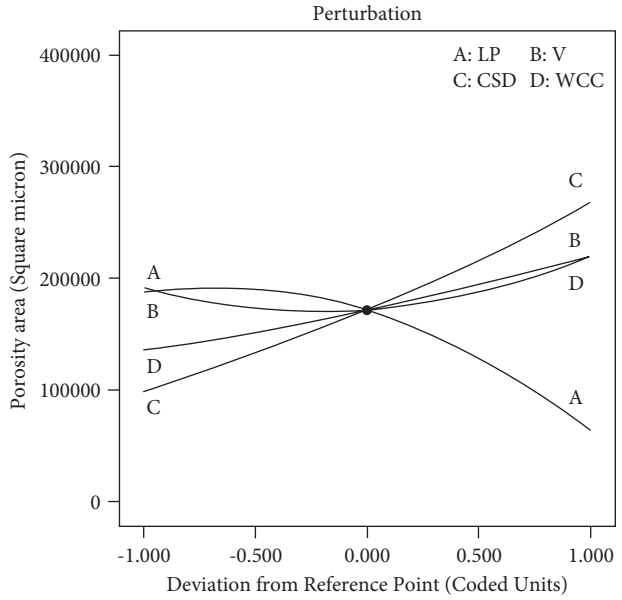

Figure 5: Perturbation diagram of the porosity area by process parameters.

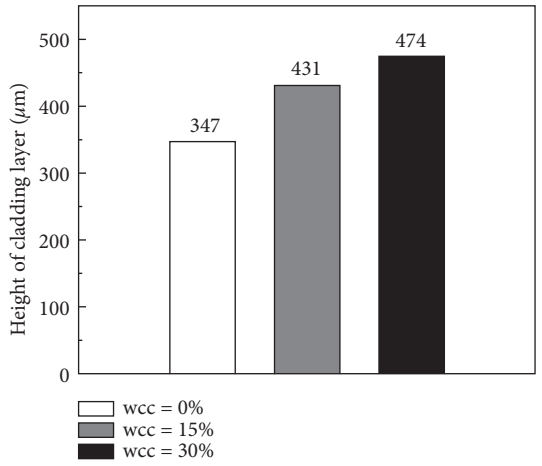

Figure 6: Influence of the WC powder content on the cladding layer height.

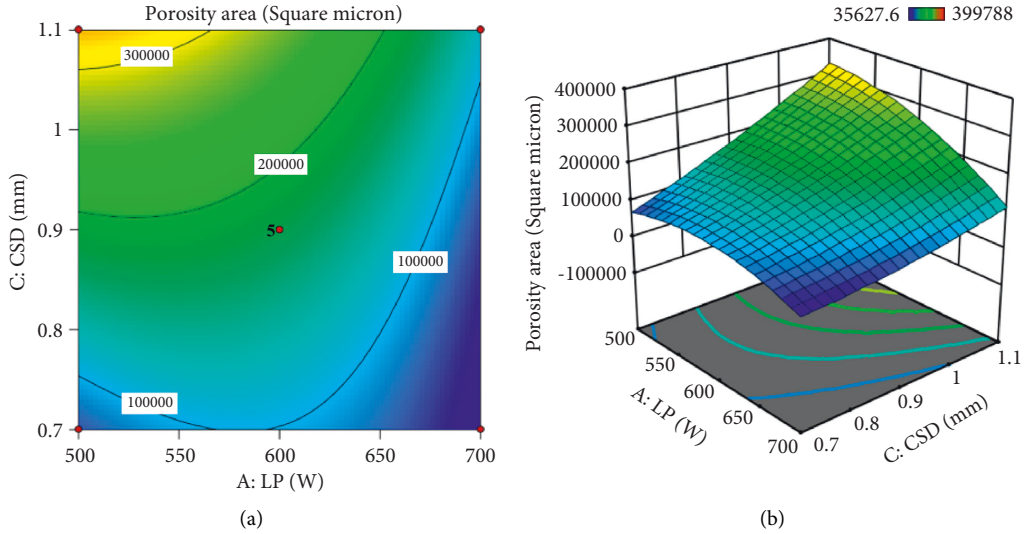

Figure 7: Effect of the interaction between the laser power and the cladding step on the porosity area: (a) contour map; (b) three-dimensional response curve.

Table 6: Variance analysis of the surface flatness.

Source	Sum of squares	Df	Mean square	F	P	
Model	0.2961	14	0.0211	2.59	0.0429	Significant
LP	0.0789	1	0.0789	9.66	0.0077	
V	0.0320	1	0.0320	3.92	0.0676	
CSD	0.0493	1	0.0493	6.04	0.0277	
WCC	0.0263	1	0.0263	3.22	0.0942	
Residual	0.1143	14	0.0082			
Lack of fit	0.0610	10	0.0061	0.4578	0.8558	Not significant
Pure error	0.0533	4	0.0133			
Correlation total	0.4104	28				
R^2	0.7215			Adeq precision	5.2830	

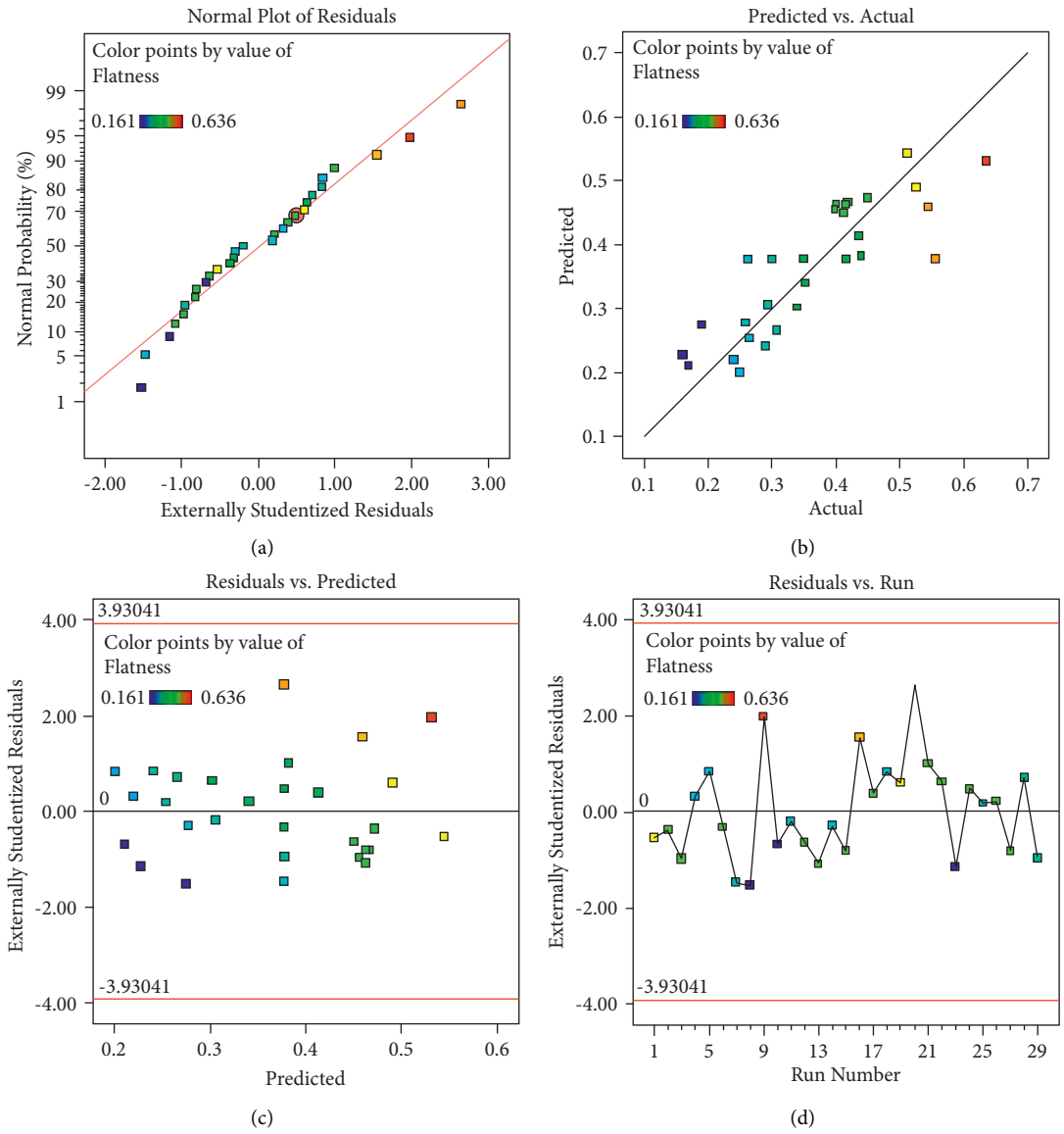

Figure 8: Surface flatness model diagnosis diagrams: (a) the normal distribution of residuals; (b) projected and actual values; (c) predicted values and residuals; (d) serial number and residuals.

each factor had the most effect on the hardness of the cladding layer, followed by the laser power. The scanning speed had a significant effect on the hardness. Although the cladding step had no significant effect on the hardness of the cladding layer, the second-order cladding step had a significant effect on the hardness of the cladding layer. In

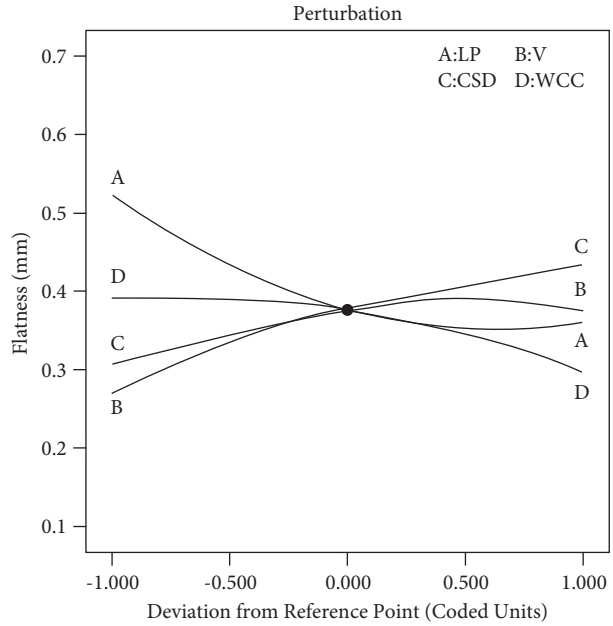

Figure 9: Perturbation diagram of the process parameters on the surface flatness.

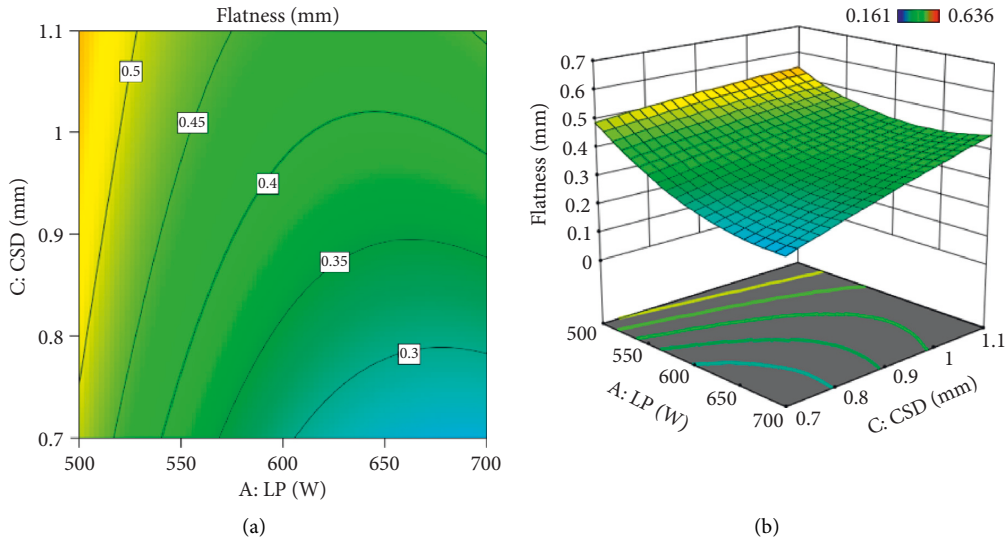

Figure 10: Influence of the interaction between the laser power and the cladding step on surface flatness: (a) contour map; (b) three-dimensional response curve.

addition, the second-order laser power and the second-order WC powder content also had a significant effect on the hardness of the cladding layer.

As can be seen from Figure 11(a), most of the residual values of the regression model are distributed around 0, indicating that the residual values of the model conform to the normal distribution and the model construction is reasonable. In Figure 11(b), the predicted values of the model fit the actual values well, which indicates that the prediction accuracy of the model is high and the predicted values are credible. Figure 11(c) reflects the distribution of the residual values. It can be seen that the residual values are distributed randomly without periodicity or regularity, which confirms the rationality of the model hypothesis and the reliability of the data. As can be seen from the serial number and the residual values in Figure 11(d), all the measured sample points are within a reasonable range without any outlying values, indicating good stability of the model.

3.4.2. Influence of the Laser Process Parameters on the Hardness of the Cladding Layer. Figure 12 shows the influence of various process parameters on the hardness of the cladding layer. The experimental results show that an increase in the content of WC powder is positively correlated

Table 7: Variance analysis of the hardness of the cladding layer.

Source	Sum of squares	df	Mean square	F	P	
Model	241300.00	14	17232.22	25.92	<0.0001	Significant
LP	10574.10	1	10574.10	15.87	0.0014	
V	3281.54	1	3281.54	4.94	0.0433	
CSD	7.76	1	7.76	0.01	0.9155	
WCC	212600.00	1	212600.00	319.88	<0.0001	
LP^2	5540.81	1	5540.81	8.34	0.0119	
CSD^2	3904.83	1	3904.83	5.87	0.0295	
WCC^2	5056.60	1	5056.60	7.61	0.0154	
Residual	9306.13	14	664.72			
Lack of fit	7986.78	10	798.68	2.42	0.2044	Not significant
Pure error	1319.35	4	329.84			
Correlation total	250600	28				
R^2	0.9629			Adeq Precision	18.2773	

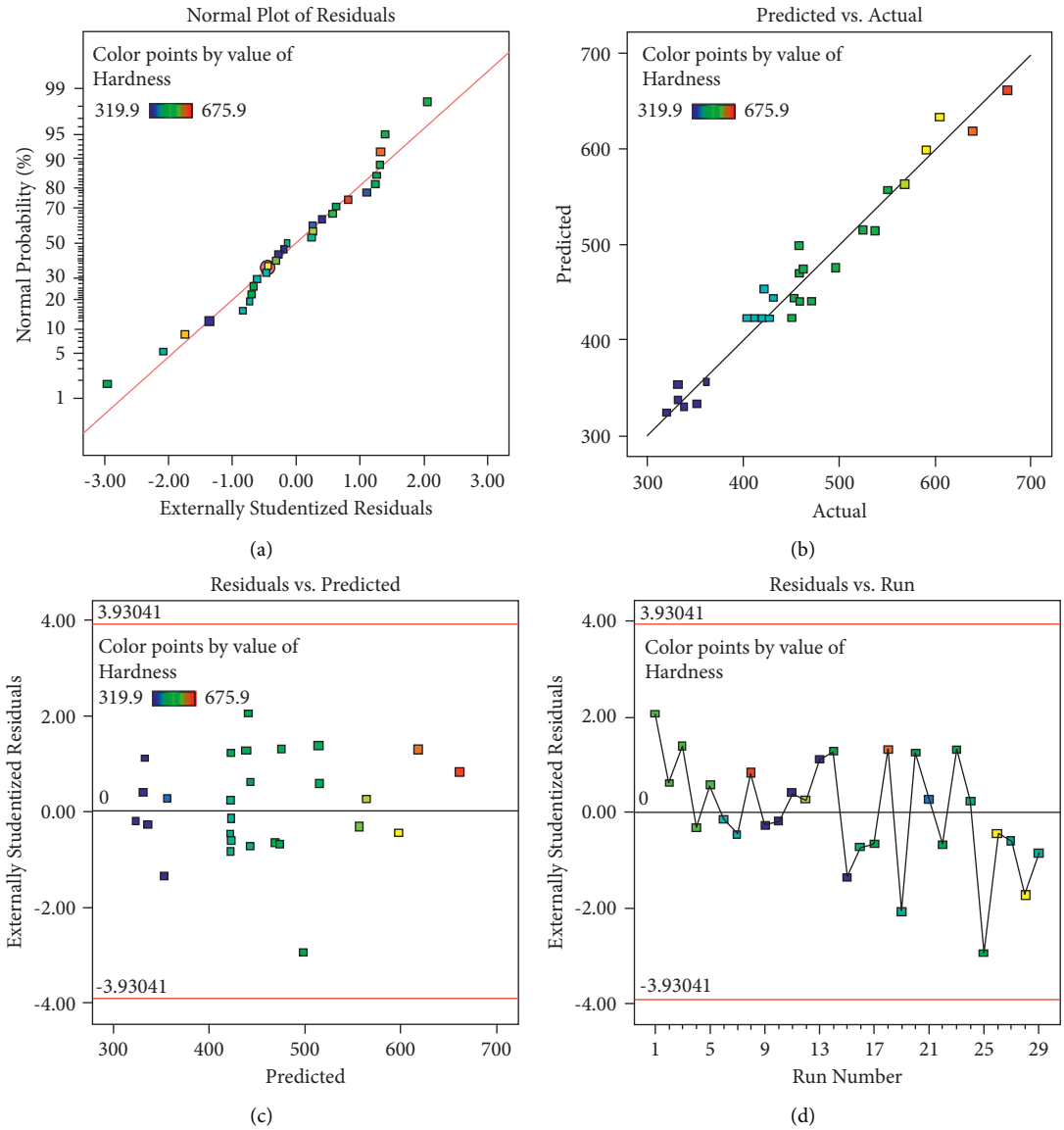

Figure 11: Diagnosis diagram of the coating hardness model. (a) The normal distribution of residuals. (b) Projected and actual values. (c) Predicted values and residuals. (d) Serial number and residuals.

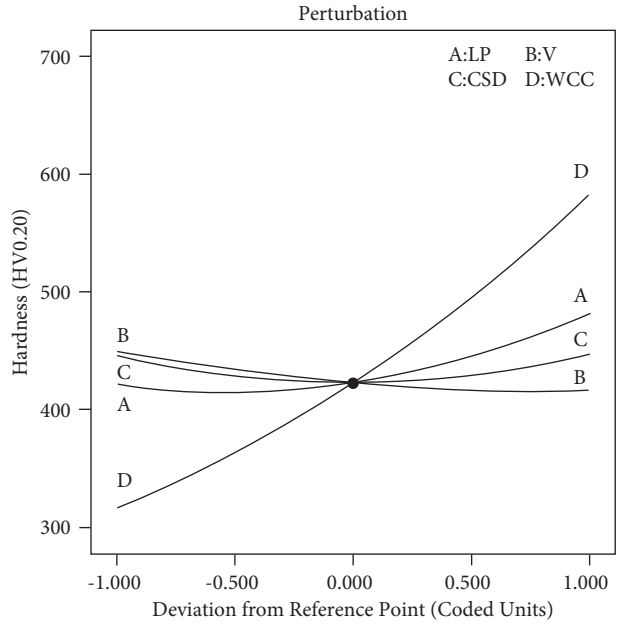

Figure 12: Perturbation diagram of the process parameters on the hardness of the cladding layer.

with the hardness of the cladding layer. This is because WC has high hardness and wear resistance. With an increase in the content of WC powder in the coating, the hardness of the coating clearly improved. At high laser power or low scanning speed, the cladding layer was formed with high hardness, which differs from previous research results [33] (the hardness of the cladding layer is inversely proportional to the laser power and proportional to the scanning speed). This is because, with an increase in the laser power or a decrease in the scanning speed, the energy density of the laser beam received by the cladding layer in unit time increases, and the ceramic powder and Co-based powder in the coating can be melted more readily, and the hardness of the coating increases. The cladding step has no significant effect on the hardness of the coating.

Figure 13 shows the influence of the interaction between the laser power and WC content on the hardness of the cladding layer. According to the analysis, when the amount of WC powder was 0%, the mass ratio of the coating powder was 10 : 0, and the coating hardness was low. With an increase in the laser power, the hardness of the cladding layer tended to be stable without significant change. When the amount of WC powder increased to 30%, the hardness of the cladding layer increased sharply, and the laser power positively correlated with the hardness of the cladding layer. These results indicate that the content of WC powder is more significant to the hardness of the coating than the laser power, and appropriately increasing the amount of WC powder and the laser power will help to enhance the hardness of the coating.

3.5. Optimization and Verification of the Process Parameters

3.5.1. Optimization Objectives. In actual working conditions, when the cladding layer is subjected to tensile stress greater than the tensile strength of the coating itself, the stress concentration is likely to occur at rigid constrained positions such as pores, resulting in cracking of the cladding layer, reducing the service life of the coating, and restricting the application of this technology to a large extent [34, 35]. The surface flatness of the coating is an important index to measure the formation quality of the cladding layer [36]. By analyzing the model of the pore area and the surface flatness, the results indicate that the laser power and the cladding step have the greatest influence on the response of these two factors. Therefore, the laser power and the cladding step were selected as the optimization objectives in this study, and the specific optimization scheme is shown in Table 8.

3.5.2. Model Validation. A set of optimal process parameters was obtained through parameter optimization, as shown in Table 9. The laser power was 700 W, the scanning speed was 300 mm/min, the cladding step was 0.7 mm, and the amount of WC was 15%. Experimental verification showed that the average error between the predicted and actual values of the porosity area, flatness, and hardness was 4.7%, 4.5%, and 5.4%, respectively, which confirms that the model has good accuracy. The model can be used to predict and optimize the process parameters of Co-based WC composite coating. In addition, the average porosity area of the optimized Co-based tungsten carbide composite coating section is 37,320 μm^2. Compared with the No. 16 sample, the porosity area decreased by 90.7%, and the average surface flatness was 0.252 mm. Compared with the No. 26 sample, the flatness decreased by 54.7%. In summary, the quality of the optimized composite coating was significantly improved. Figure 14 depicts the cross-sectional morphology of the cladding layer in the verification group, where *a*, *b*, and *c* are the cross-sectional morphology of the cladding layer in the verification group, and *e* is the pore morphology after local amplification in the verification group.

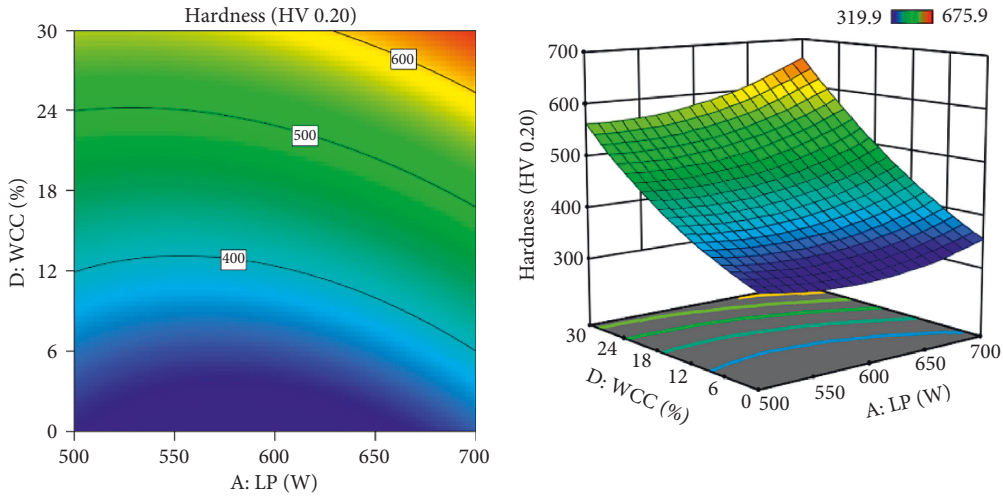

Figure 13: Influence of the interaction between laser power and WC content on the hardness of the cladding layer: (a) contour map; (b) three-dimensional response curve.

Table 8: Optimization objectives and scheme.

Name	Criteria	Lower	Upper	Importance
LP (W)	Maximize	500	700	5
V (mm/min)	In range	200	400	3
CSD (mm)	Minimize	0.7	0.9	5
WCC (%)	In range	0	30	3
Porosity area (μm^2)	In range	35627.6	399788	3
Flatness (mm)	In range	0.161	0.636	3
Hardness (HV 0.2)	In range	319.9	675.9	3

Table 9: Model prediction and validation.

	LP (W)	V (mm/min)	CSD (mm)	WCC (%)	Porosity area (μm^2)	Flatness (mm)	Hardness (HV 0.2)	Desirability	
Prediction	700	300	0.7	15	36319	0.254	498.2	1.000	Selected
	700	300	0.7	15	37332	0.268	471.0		
Experiment	700	300	0.7	15	35282	0.250	455.0		
	700	300	0.7	15	39375	0.238	487.8		
Average error					4.7%	4.5%	5.4%		

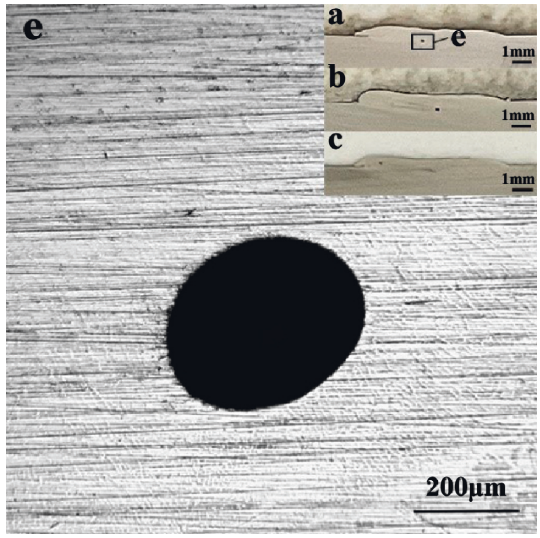

Figure 14: Cross-sectional morphology and partial enlargement of the cladding layer.

4. Conclusion

In this study, based on laser cladding technology, a mathematical model between the response and process parameters of multilap Stellite 6/WC composite coatings was established by RSM, and the model was optimized. Through variance and residual analysis, the following conclusions can be drawn:

(1) The cladding step and the laser power are the most significant factors affecting the porosity area and the surface flatness of the cladding layer, while the WC content is the most significant parameter affecting the hardness of the coating.

(2) With increasing laser power, the cladding layer's porosity area and surface flatness decrease, while the microhardness increases. The scanning speed has little effect on the porosity area and the surface flatness and is negatively correlated with the coating hardness. All these factors increased with an increase in the cladding step. With increasing WC content, the porosity area and coating hardness increase, and the surface flatness tends to level out.

(3) Increasing the laser power and decreasing the cladding step are beneficial to the suppression of the porosity area and surface flatness of the cladding layer, and the interaction between high laser power and high WC content can enhance the hardness of the coating.

(4) The optimal combination of process parameters is a laser power of 700 W, a scanning speed of 300 mm/min, a cladding step of 0.7 mm, and WC content of 15%. The average error between the predicted and the experimental values was less than 6%.

Data Availability

The data used to support the findings of this study are included within the article. Further dataset or information is available from the corresponding authors upon request.

Conflicts of Interest

The authors declare that they have no conflicts of interest.

Acknowledgments

This study was supported by the National Natural Science Foundation of China (Grant no. 62073089), the Special Project for Key Fields of Higher Education in Guangdong Province (Grant no. 2020ZDZX2061), and the Postgraduate Education Innovation Project of Guangdong Ocean University (Grant no. 040502112103).

References

[1] L. W. Lu, T. M. Liu, M. J. Tan, J. Chen, and Z. C. Wang, "Effect of annealing on microstructure evolution and mechanical property of cold forged magnesium pipes," *Materials and Design*, vol. 39, pp. 131–139, 2012.

[2] C. Katinas, T. Throop, Y. C. Shi, and A. Frank, "Laser cladding of Stellite-6 with a coaxial nozzle via modeling and systematic experimental investigations," *International Journal of Advanced Manufacturing Technology*, vol. 113, pp. 837–853, 2021.

[3] Y. Chen, T. M. Liu, L. W. Lu, and Z. C. Wang, "Thermally diffused antimony and zinc coatingson magnesium alloys AZ31," *Surface Engineering*, vol. 28, no. 5, pp. 382–386, 2012.

[4] L. J. Song, G. C. Zeng, H. Xiao, X. F. Xiao, and S. M. Li, "Repair of 304 stainless steel by laser cladding with 316L stainless steel powders followed by laser surface alloying with WC powders," *Journal of Manufacturing Processes*, vol. 24, pp. 116–124, 2016.

[5] Y. Chen, L. B. Hu, C. J. Qiu, and Z. C. Wang, "Effects of carbon and boron on structure and properties of austenitic stainless steel coatings fabricated by laser remanufacturing," *Steel Research International*, vol. 90, Article ID 1800473, pp. 1–9, 2019.

[6] M. Froend, S. Riekehr, N. Kashaev, B. Klusemann, and J. Enz, "Process development for wire-based laser metal deposition of 5087 aluminium alloy by using fibre laser," *Journal of Manufacturing Processes*, vol. 34, pp. 721–732, 2018.

[7] Y. Zhao, C. Guan, L. Y. Chen, J. Y. Sun, and T. B. Yu, "Effect of process parameters on the cladding track geometry fabricated by laser cladding," *Optik*, vol. 223, Article ID 165447, 2020.

[8] L. S. Shu, B. Wang, and Y. Y. He, "Optimization of Process Parameters of Laser Cladding 304L Alloy Powder Based on Orthogonal Experiment," *Mechanical Engineering Science*, vol. 1, no. 2, pp. 18–24, 2020.

[9] U. D. Oliveira, V. Ocelı´k, and J. T. M. D. Hosson, "Analysis of coaxial laser cladding processing conditions," *Surface and Coatings Technology*, vol. 197, pp. 127–136, 2005.

[10] G. C. Onwubolu, J. P. Davim, C. Oliveira, and A. Cardoso, "Prediction of clad angle in laser cladding by powder using response surface methodology and scatter search," *Optics & Laser Technology*, vol. 39, no. 6, pp. 1130–1134, 2007.

[11] H. M. Liu, X. P. Qin, S. Huang, Z. Q. Hu, and M. Ni, "Geometry modeling of single track cladding deposited by high power diode laser with rectangular beam spot," *Optics and Lasers in Engineering*, vol. 100, pp. 38–46, 2018.

[12] A. Khorram, A. D. Jamaloei, M. Paidar, and X. J. Cao, "Laser cladding of Inconel 718 with 75Cr3C2 + 25(80Ni20Cr) powder: statistical modeling and optimization," *Surface and Coatings Technology*, vol. 378, Article ID 124933, 2019.

[13] Y. Liu, C. Liu, W. S. Liu et al., "Optimization of parameters in laser powder deposition AlSi10Mg alloy using Taguchi method," *Optics & Laser Technology*, vol. 111, pp. 470–480, 2019.

[14] L. L. Shi, J. T. Zhou, H. Li et al., "Evolution of multi pores in Ti6Al4V/AlSi10Mg alloy during laser post-processing," *Materials Characterization*, vol. 176, Article ID 111109, 2021.

[15] I. Tabernero, A. Lamikiz, S. Martı´nez, E. Ukar, and J. Figueras, "Evaluation of the mechanical properties of Inconel 718 components built by laser cladding," *International Journal of Machine Tools and Manufacture*, vol. 51, pp. 465–470, 2011.

[16] Y. Hu, L. Wang, J. H. Yao, H. C. Xia, J. H. Li, and R. Liu, "Effects of electromagnetic compound field on the escape behavior of pores in molten pool during laser cladding," *Surface and Coatings Technology*, vol. 383, Article ID 125198, 2020.

[17] T. Fu, X. H. Peng, C. Wan et al., "Molecular dynamics simulation of plasticity in VN(001) crystals under

nanoindentation with a spherical indenter," *Applied Surface Science*, vol. 392, pp. 942–949, 2017.

[18] T. Fu, X. H. Peng, X. Chen et al., "Molecular dynamics simulation of nanoindentation on Cu/Ni nanotwinned multilayer films using a spherical indenter," *Scientific Reports*, vol. 6, Article ID 35665, 2016.

[19] T. Fu, X. H. Peng, C. Huang, D. Q. Yin, Q. B. Li, and Z. C. Wang, "Molecular dynamics simulation of VN thin films under indentation," *Applied Surface Science*, vol. 357, pp. 643–650, 2015.

[20] Y. Chen, L. B. Hu, C. J. Qiu, B. He, and Z. C Wang, "Effects of helium ion irradiation on properties of crystalline and amorphous multiphase ceramic coatings," *Journal of Materials Engineering and Performance*, vol. 26, pp. 4131–4137, 2017.

[21] Y. Zhang, C. J. Qiu, Y. Chen et al., "Influence of high-frequency micro-forging on microstructure and properties of 304 stainless steel fabricated by laser rapid prototyping," *Steel Research International*, vol. 84, pp. 870–877, 2013.

[22] Z. Y. Jia, W. J. Wang, Z. C. Li et al., "Morphology-tunable synthesis of intrinsic room-temperature ferromagnetic γ-Fe2O3 nanoflakes," *ACS Applied Materials & Interfaces*, vol. 13, pp. 24051–24061, 2021.

[23] Z. C. Wang, W. Zeng, L. Gu, M. Saito, S. Tsukimoto, and Y. Ikuhara, "Atomic-scale structure and electronic property of the LaAlO3/TiO2 interface," *Journal of Applied Physics*, vol. 108, Article ID 113701, 2010.

[24] D. Q. Yin, X. H. Peng, Y. Qin, and Z. C. Wang, "Electronic property and bonding configuration at the TiN(111)/VN(111) interface," *Journal of Applied Physics*, vol. 108, Article ID 033714, 2010.

[25] Y. Liu, J. Zhang, Z. C. Pang, and W. H. Wu, "Investigation into the influence of laser energy input on selective laser melted thin-walled parts by response surface method," *Optics and Lasers in Engineering*, vol. 103, pp. 34–45, 2018.

[26] H. Vahiddastjerdia, A. Rezaeiana, M. R. Toroghinejada, G. Dinib, and E. Ghassemali, "Optimizing pulsed Nd: YAG laser welding of high-Mn TWIP steel using response surface methodology technique," *Optics & Laser Technology*, vol. 120, Article ID 105721, 2019.

[27] Y. W. Sun and M. Z. Hao, "Statistical analysis and optimization of process parameters in Ti6Al4V laser cladding using Nd: YAG laser," *Optics and Lasers in Engineering*, vol. 50, pp. 985–995, 2012.

[28] W. Y. Gao, S. S. Zhao, F. L. Liu, Y. B. Wang, C. Y. Zhou, and X. C. Lin, "Effect of defocus manner on laser cladding of Fe-based alloy powder," *Surface and Coatings Technology*, vol. 248, pp. 54–62, 2014.

[29] D. Wang, Y. Q. Yang, X. B. Su, and Y. H. Chen, "Study on energy input and its influences on single-track, multi-track, and multi-layer in SLM," *International Journal of Advanced Manufacturing Technology*, vol. 58, pp. 1189–1199, 2012.

[30] Z. Maswuma and A. P. Popoola, "The effect of process parameters on the hardness and wear resistance performance of laser cladded Ti-Si coatings on Ti-6Al-4V alloy," *International Journal of Microstructure and Materials Properties*, vol. 14, no. 1, pp. 1–13, 2019.

[31] Y. Javid, "Multi-response optimization in laser cladding process of WC powder on Inconel 718," *CIRP Journal of Manufacturing Science and Technology*, vol. 31, pp. 406–417, 2019.

[32] D. Bartkowski, A. Bartkowska, and P. Jurči, "Laser cladding process of Fe/WC metal matrix composite coatings on low carbon steel using Yb: YAG disk laser," *Optics & Laser Technology*, vol. 136, Article ID 106784, 2021.

[33] G. R. Meng, L. D. Zhu, J. D. Zhang, Z. C. Yang, and P. S. Xue, "Statistical analysis and multi-objective process optimization of laser cladding TiC-Inconel718 composite coating," *Optik*, vol. 240, Article ID 166828, 2021.

[34] L. W. Lu, T. M. Liu, Y. Chen, and Z. C. Wang, "Deformation and fracture behavior of hot extruded Mg alloys AZ31," *Materials Characterization*, vol. 67, pp. 93–100, 2012.

[35] K. Qi, Y. Yang, R. Sun et al., "Effect of magnetic field on crack control of Co-based alloy laser cladding," *Optics & Laser Technology*, vol. 141, Article ID 107129, 2021.

[36] C. R. Chen, G. F. Lian, J. B. Jiang, and Q. T. Wang, "Simplification and experimental investigation of geometrical surface smoothness model for multi-track laser cladding processes," *Journal of Manufacturing Processes*, vol. 36, pp. 621–628, 2018.